Paramagnetic susceptibility simulations from crystal field effects on Nd^{3+} in $AgNd(WO_4)_2$

C. Colón[a] and A. Alonso-Medina
Departamento de Física Aplicada. E.U.I.T. Industrial-UPM, Ronda de Valencia 3, 28012 Madrid, Spain

J. Montero and F. Fernandez
Departamento de Química Industrial y Polímeros, E.U.I.T. Industrial-UPM, Ronda de Valencia 3, 28012 Madrid, Spain

C. Cascales
Instituto de Ciencia de Materiales de Madrid, CSIC, Cantoblanco, 28049 Madrid, Spain

(Received 11 June 2003; accepted 25 September 2003)

Polycrystalline $AgNd(WO_4)_2$ has been prepared by a in solid-state reaction. X-ray diffraction measurements indicate that this compound crystallizes with a scheelite-type tetragonal structure. Absorption and emission spectra have been measured, using the technique of the crystal field parameters, to obtain the energy levels scheme for Nd^{3+} ions in the crystalline matrix. These data indicate the existence of a structural local disorder associated with a random distribution of the ions of Ag^+ and Nd^{3+}. The temperature variation of the paramagnetic susceptibility in the range from 2 to 300 K has been studied. The Van Vleck formula has been used to calculate the temperature variation of the paramagnetic susceptibility and it was compared with the experimental results. Particularly at low temperatures, satisfactory agreement has been obtained. © *2003 American Institute of Physics.* [DOI: 10.1063/1.1627322]

I. INTRODUCTION

Recently, the preparation, structure, luminescence, and the magnetic properties of $ALn(XO_4)_2$ (A=monovalent alkali, Cu and Ag; Ln=divalent lanthanide; X=Mo, W) have been studied. Depending on their composition, they present a very wide diversity of crystal structure types.[1–19] Most of these compounds have the orthorhombic structure,[5–9] but some have a completely different structure and crystallize in the triclinic system,[8,10–12] in the monoclinic system,[4,13–15] or in the tetragonal system.[16–19]

In the tungstate family, two structural types are found depending on the ionic radius of the lanthanide: $AgLa(WO_4)_2$ is tetragonal S.G. $I4_1/a$ (No. 88)[20] and a more recent work[4] on $AgLn(WO_4)_2$ (Ln=Eu, Gd, Tb, and Dy) shows that the crystal structure of these compounds can be deduced from the tetragonal scheelite by a monoclinic distortion of the scheelite unit cell to accommodate the smaller Ln^{3+}.

This work reports on the preparation, crystal structure, and spectroscopic and magnetic properties of $AgNd(WO_4)_2$. At first glance, x-ray data can be interpreted using the S.G. $I4_1/a$ (No. 88) tetragonal scheelite structure.

II. EXPERIMENT

Polycrystalline $AgNd(WO_4)_2$ was prepared by solid-state reaction in air using stoichiometric amounts of Ag_2O, Nd_2O_3, and WO_3, heated at 800 K in ceramic crucible. The crystal structure and purity of the sample were tested by x-ray diffraction. The refinement was performed in the tetragonal space S.G. $I4_1/a$ (No. 88) and used the starting values for the unit-cell and positional parameters reported for the $NaNd(WO_4)_2$.[20] The x-ray pattern was measured using Cu $K\alpha$ radiation ($\lambda=1.540\,598$ Å) with a Siemens D500 diffractometer equipped with a graphite monochromator. Data were collected at 300 K over an angular range of $5\leqslant 2\theta\leqslant 110°$, scanning in steps of 0.05°, and a counting time of 10 s per step. The results were analyzed by the Rietveld profile refinement method, using a strongly modified version[21] of the Wiles and Young program.

The infrared spectrum of the sample was determined in the region of 1000–400 cm^{-1} using a Perkin–Elmer Fourier transform infrared spectrometer. Optical absorption measurements at 9 K were obtained using a CARY 5E spectrometer as far as 29 000 cm^{-1}. The luminescence, excited by a Spectra Physics Ar^+-Kr^+ laser using the 28 490 cm^{-1} UV line, was detected at 5 K using a double HR-460 Jobin–Yvon monochromator with a charge coupled device detector. A superconducting quantum interference device magnetometer (Quantum Design) operating from 300 to 1.5 K at 1000 Oe was used to perform the paramagnetic susceptibility measurements.

III. ENERGY LEVEL SCHEME SIMULATION

The method used to calculate the energy levels of the Nd^{3+} in its crystalline environment is based in the central field approximation.

The total Hamiltonian[22] consists of two parts,

$$H=H_{\mathrm{FI}}+H_{\mathrm{CF}},$$

[a]Electronic mail: ccolonh@fais.upm.es

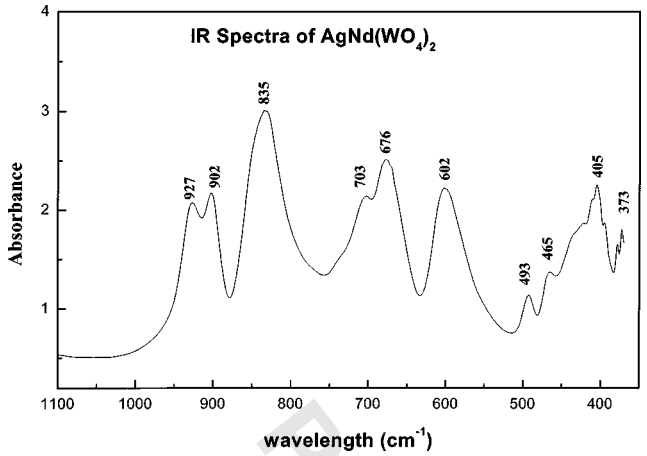

FIG. 1. Infrared spectrum at 300 K for $AgNd(WO_4)_2$.

H_{FI} is the free ion part, which includes the spherically symmetric one-electron term of the Hamiltonian, the electrostatic repulsion between equivalent f electrons, the spin–orbit interaction, and term accounting for higher-order corrections (configuration interaction, spin-other-orbit, and spin–spin interactions, and the electrostatically correlated spin–orbit interactions).[22] For the $4f^3$ configuration of Nd^{3+} the T^k parameters, representing non-negligible three-body interactions are introduced although some of them are fixed to values used in earlier studies

$$H_{\mathrm{FI}}=H_0+\sum_{k=0,1,2,3}E^K e_k+\zeta_{4f}A_{\mathrm{SO}}+\alpha L(L+1)+\beta G(G_2)+\gamma G(R_2)+\sum_{k=2,4,6}P^k p_k+\sum_{k=0,2,4}M^k m_k++\sum_{k=2,3,4,6,7,8}T^k t_k, \quad (1)$$

where H_{CF} is the crystal field term, which takes into account the effect of the electrostatic interactions arising from the surrounding ions of the f electrons. In the presence of a crystalline electric field, the degeneracy of each state of the free ion will be lifted according to the site symmetry of the rare-earth ion in the crystal lattice. Following Wybourne's formalism[23] the crystal field Hamiltonian is expressed as a sum of products of spherical harmonics and B_q^k crystal field parameters CFPs:

$$H_{\mathrm{CF}}=\sum_{k=2}^{4,6}\sum_{q=0}^{k}[\mathrm{Re}(B_q^k)(C_q^k+(-1)^q C_{-q}^k)+i\,\mathrm{Im}(B_q^k)(C_q^k-(-1)^q C_{-q}^k)]. \quad (2)$$

In the tungstate lattice, the Nd occupies a crystallographic position with the C_2 point symmetry. The series representation of the CFP has 14 nonzero parameters among which only five $\mathrm{Im}(B_q^k)$, since $\mathrm{Im}(B_2^2)$ is set to zero by an appropriate choice of the reference axis system.

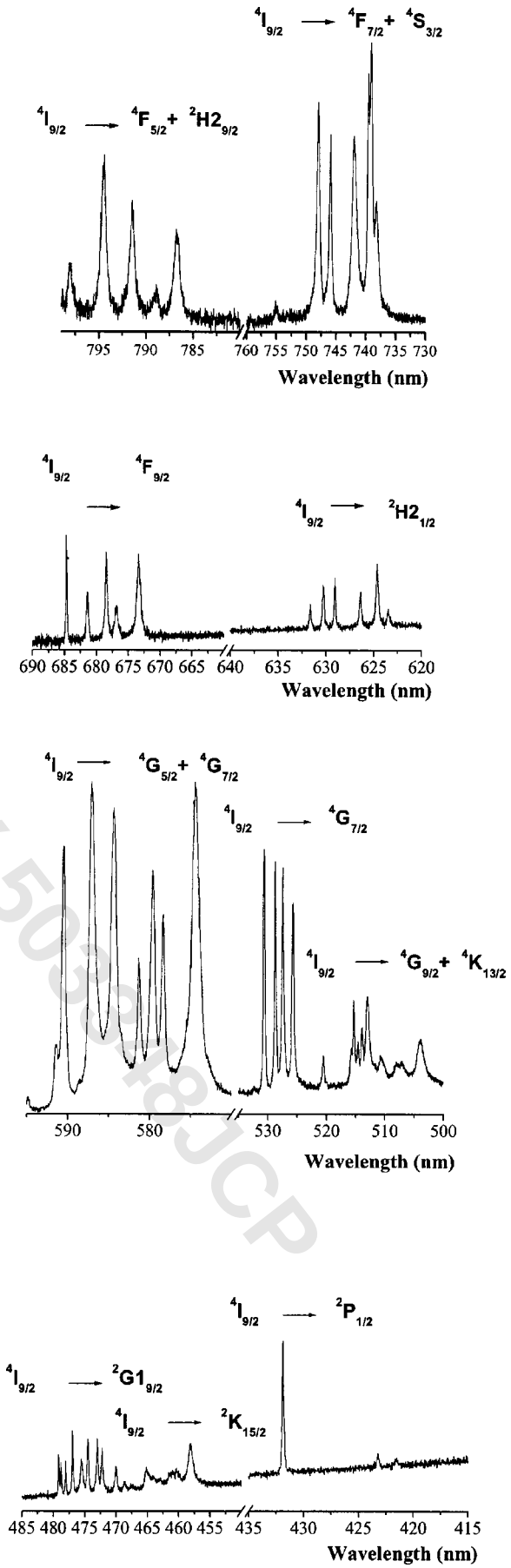

FIG. 2. Absorption spectra for Nd^{3+} in $AgNd(WO_4)_2$ at 9 K.

TABLE I. Observed and calculated energy levels (cm^{-1}) of the Nd^{3+} ion in $AgNd(WO_4)_2$.

$^{2s+1}L_i$	Observed	Calculated	Δ	$^{2s+1}L_i$	Observed	Calculated	Δ
$^4I_{9/2}$	0	−17	17	$^4G_{5/2}$	17 110	17 108	2
	78	62	16	$^4G_{7/2}$	17 205	17 208	−3
	220	211	9		17 254	17 252	2
	244	259	−15	$^4G_{5/2}$	17 291	17 285	6
	434	434	0		17 412	17 440	−28
$^4I_{11/2}$	1913	1924	−110	$^4G_{7/2}$	18 846	18 835	11
	1962	1957	5		18 911	18 900	11
	2032	2029	3		18 960	18 977	−17
	2062	2067	−5		19 019	19 024	−5
	2169	2168	1	$^4G_{9/2}$		19 309	
	2187	2191	−4		19 393	19 390	3
$^4I_{13/2}$	3876	3872	4		19 408	19 403	5
	3914	38994	15	$^2K_{13/2}$	19 435	19 435	0
	3954	3976	−22	$^4G_{9/2}$	19 461	19 464	−3
	4011	4009	2		19 491	19 499	−8
	4140	4132	8		19 539	19 518	21
		4159		$^2K_{13/2}$		19 651	
		4184				19 696	
$^4I_{15/2}$		5807				19 761	
		5852				19 886	
		5994				19 978	
		6013		$^2Gl_{9/2}$	20 869	20 847	22
		6170			20 881	20 897	−16
		6266			20 914	20 909	5
		6318			20 962	20 949	13
		6351			21 028	21 021	7
$^4F_{3/2}$	11 389	11 402	−13	$^2Dl_{3/2}$	21 074	21 086	−12
	11 488	11 483	5		21 136	21 132	4
$^4F_{5/2}$	12 416	12 395	21	$^4G_{11/2}$	21 170	21 193	−23
	12 458	12 440	18		21 277	21 291	−14
$^2H2_{9/2}$	12 485	12 528	−43		21 339	21 332	7
	12 531	12 555	−24.	$^2K_{15/2}$		21 461	
$^4F_{5/2}$	12 586	12 569	17		21 498	21 493	5
$^2H2_{9/2}$	12 634	12 623	11	$^4G_{11/2}$	21 550	21 555	−5
	12 711	12 684	27	$^2K_{15/2}$		21 630	
		12 719				21 673	
$^4F_{7/2}$	13 368	13 372	−4	$^4G_{11/2}$	21 694	21 683	11
	13 405	13 426	−21		21 725	21 712	13
$^4S_{3/2}$	13 478	13 495	−17	$^2K_{15/2}$		21 763	
	13 523	13 507	16		21 827	21 831	−4
$^4F_{7/2}$	13 531	13 527	4			21 876	
		13 551				21 965	
$^4F_{9/2}$	14 604	14 624	−20	$^2P_{1/2}$	23 155	23 148	7
	14 675	14 656	19	$^2D1_{5/2}$	23 630	23 626	4
	14 740	14 720	20		23 722	23 725	−3
	14 774	14 792	−18			23 817	
	14 849	14 855	−6	$^2P_{3/2}$		26 032	
$^2H2_{11/2}$	15 865	15 865	0			26 130	
	15 832	15 872	−40	$^4D_{3/2}$	27 739	27 720	19
	15 894	15 892	2		27 800	27 811	−11
		15 908			27 987	27 988	−1
		15 910		$^4D_{5/2}$	28 106	28 090	16
	15 963	15 950	13			28 302	
$^4G_{5/2}$	16 936	16 944	−8	$^4D_{1/2}$	28 430	28 448	−18
	17 039	17 037	2				

A set of phenomenological CFPs for $AgGd_{1-x}Eu_x(WO_4)_2$ ($x=0.05$) previously determined on the basis of 16 observed $^7\mathbf{F}_{0-5}$ energy levels in the C_{2v} symmetry, and involving only nine real CFPs is the most convenient set of starting values for crystal field calculations[24]

The least-square refinements between the experimental and calculated energy levels values were carried out by minimizing the root-mean-square function σ defined as

$$\sigma=\left[\sum \left(E_{\text{exp}}-E_{\text{cal}}\right)^2/\left(N_{\text{lev}}-N_{\text{par}}\right]^{1/2}, \tag{3}$$

where E_{exp} and E_{cal} are the experimental and calculated energies, respectively, N_{lev} is the number of experimental levels and N_{par} is the number of parameters.

The simulations were performed by the program IMAGE99.[25]

TABLE II. Free ion and CFPs (cm^{-1}) for Nd^{3+} in $AgNd(WO_4)_2$.

Parameter	Value (cm^{-1})
E^0	23 453(1)
E^1	4831.6(0.8)
E^2	23.49(0.02)
E^3	484.65(0.09)
α	25.53(0.05)
β	−774(4)
γ	[1500]
ζ	875.2(0.7)
T^2	[298]
T^3	29(2)
T^4	81(2)
T^6	−253(6)
T^7	291(7)
T^8	[305]
M^0	1.38(0.08)
M^2	.80
M^4	.53
P^2	171(16)
P^4	96
P^6	64
$\mathrm{Re}(B_0^2)$	546(23)
$\mathrm{Re}(B_2^2)$	154(19)
$\mathrm{Re}(B_0^4)$	−1296(41)
$\mathrm{Re}(B_2^4)$	725(33)
$\mathrm{Re}(B_4^4)$	−456(48)
$\mathrm{Re}(B_0^6)$	−372(50)
$\mathrm{Re}(B_2^6)$	−2(69)
$\mathrm{Re}(B_4^6)$	−472(55)
$\mathrm{Re}(B_6^6)$	−10(78)
$\mathrm{Im}(B_0^2)$	.00
$\mathrm{Im}(B_2^2)$	.00
$\mathrm{Im}(B_0^4)$	.00
$\mathrm{Im}(B_2^4)$	−38(90)
$\mathrm{Im}(B_4^4)$	−857(30)
$\mathrm{Im}(B_0^6)$	.00
$\mathrm{Im}(B_2^6)$	−148(85)
$\mathrm{Im}(B_4^6)$	−536(44)
$\mathrm{Im}(B_6^6)$	−256(58)
Number of levels	79
σ	17.4
Residue	15824

Notes: Values in parentheses refer to estimated standard deviations in the indicated parameter. Values in square brackets were not allowed to vary in the parameter fitting. M^0, M^2, M^4 were constrained by the ratios $M^2 = 0.5625\, M^0$, $M^4 = 0.3125\, M^0$ (see Ref. 31). P^2, P^4, P^6 were constrained by the ratios $P^4 = 0.75\, P^2$, $P^6 = 0.50\, P^2$ (see Ref. 31).

IV. MAGNETIC SUSCEPTIBILITY AND CRYSTAL FIELD LEVELS

An applied external magnetic field constitutes an interaction operating as a perturbation of the system. In fact, due to the relatively small used magnetic field, the best way to calculate the magnetic susceptibility is to use the Van Vleck formula.[26,27] The susceptibility corresponding to a principal axis $i(=x,y,z)$ is given by

$$\chi^{(i)} = N\beta^2 \sum_a \left[\frac{\langle \phi_a | (L + g_e S)\cdot u | \phi_a \rangle^2}{kT} - 2\sum_b \frac{\langle \phi_a | (L + g_e S)\cdot u | \phi_b \rangle \langle \phi_b | (L + g_e S)\cdot u | \phi_a \rangle}{E_a - E_b} \right] \times B_a \tag{4}$$

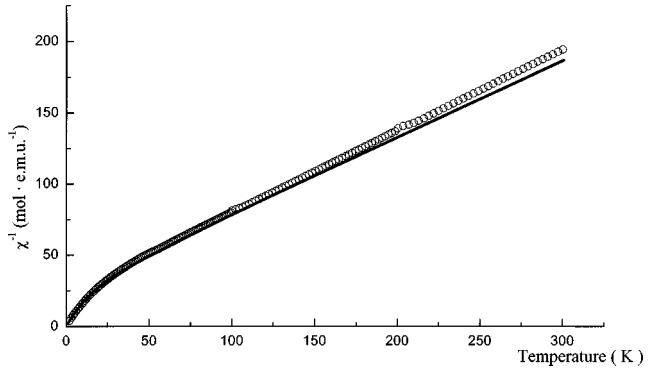

FIG. 3. Comparison between experimental (symbols) and calculated temperature dependence of χ_m^{-1} for $AgNd(WO_4)_2$.

where N is Avogadro number, β is the Bohr magneton, k is the Boltzmann constant, E and ϕ are the nonperturbed energy levels and wave functions, respectively, described on $|SLJM_J\rangle$ basis, and $L + g_e S$ is the component (i) of the magnetic interaction associated to a tensorial operator of rank 1, the magnetic dipole operator, with u as the unitary vector corresponding to the i axis. The sums run over all thermally populated levels according to the Boltzman distribution

$$B_a = \exp\left(\frac{-E_a}{kT}\right) \Big/ \sum_a \exp\left(\frac{-E_a}{kT}\right). \tag{5}$$

The average paramagnetic susceptibility for a low-symmetry polycrystalline powder is given by $\chi_{\mathrm{av}} = (\chi_x + \chi_y + \chi_z)/3$.

Equation (4) is the sum of a temperature-dependent diagonal term and a temperature-independent off-diagonal term, which is reminiscent of the classical Curie–Weiss law. The off-diagonal term, a result of the second-order perturbation, usually has little importance, with the exception of the ground states with $J = 0$. The sum runs over all other states $(b \neq a)$. Energy levels up to 5000 and 10 000 cm^{-1} for the diagonal and off-diagonal terms, respectively, which are largely sufficient to cover the thermal population effect above 300 K, were accounted for in the calculation along with the J mixing of the levels. For lanthanide compounds for which no magnetic interactions between the magnetic ions are detected, this calculation is in fairly good agreement with experiment results for neodymium compounds.[28,29]

Calculations of the thermal variation of χ were also performed by IMAGE99.[25]

V. RESULTS AND DISCUSSION

A. X-ray diffraction pattern

Experimental x-ray data can be explained using a tetragonal scheelite structure. Considering the discrepancies between experimental and theoretical intensities of several reflections, let us to try explain our data using a monoclinic distortion of the scheelite unit cell.[4] These trials were unsuccessful due to the absence in our data of several predicted reflections. Although an analysis of neutron diffraction is in progress in order to solve these problems, the nonexistence of the above mentioned monoclinic reflections allows this hypothesis to be discarded and to assume in a tetragonal

symmetry with some local disorder. The final cell parameters obtained were $a\,(\text{Å}) = 0.532\,\text{nm}$, $b\,(\text{Å}) = 0.532\,\text{nm}$, and $c\,(\text{Å}) = 1.158\,\text{nm}$.

B. Infrared spectra

The IR in the region of 400–1000 cm^{-1} is presented in Fig. 1. The IR spectrum for $NdAg(WO_4)_2$ is somewhat more complicated than those for similar lanthanide-containing molybdates.[20] In these compounds, the MoO_4^{2-} having S_4 site symmetry shows three absorptions in this region around 890, 820, and 420 cm^{-1}, which correspond, respectively, to the ν_1, ν_3, and ν_2 modes of tetrahedral MoO_4^{2-} group.[30] The $NdAg(WO_4)_2$ spectra are similar to those for monoclinic $DyAg(WO_4)_2$.[4] The ν_3 mode splits into four components about 832, 703, 678, and 603 cm^{-1}. The ν_1 mode presents two components about 928 and 902 cm^{-1}. The ν_2 mode appears in four components about 493, 466, 403, and 369 cm^{-1}.

C. Absorption and luminescence

Transitions in the absorption spectrum of Nd^{3+} on $NdAg(WO_4)_2$ at 9 K originate from the lowest Stark component of the $^4\mathbf{I}_{9/2}$ ground-state manifold. Several lines can be observed, Fig. 2, in the spectra. The transition between $^4I_{9/2}$ and $^2P_{1/2}$ is one such example.

The energy positions of the $^4\mathbf{I}_{9/2}$ have been established from emission spectrum. There are some intense emission lines of $^4\mathbf{F}_{3/2}$ to $^4\mathbf{I}_{9/2}$.

Based in a preliminary energy level scheme,[24] an improved pattern with 79 energy levels was considered in the simulation with C_2 symmetry.

Throughout the refinement process the γ parameter was fixed to a standard value since the levels in which its effect is important are not experimentally observed (e.g., the $^2\mathbf{F2}$ terms). For the same reason, T^2 and T^8 could not be varied freely. Although simulation with S_4 symmetry were realized, a notable improvement in the reproduction of energy levels is achieved when the $\text{Im}(B_q^k)$ parameters corresponding to C_2 symmetry are introduced. The simulation yielded energy level schemes in good agreement with the experimental data as can be seen in Table I. No large individual discrepancies between experimental and calculated energy levels are observed. The CFPs set shown in Table II. is characterized by large values of $\text{Re}(B_0^2)$, $\text{Re}(B_0^4)$ and $\text{Re}(B_0^6)$ and by stable nonzero values for the $\text{Im}(B_q^k)$ parameters.

It can be concluded from the well resolved spectra and the good agreement between experimental data and the calculated energy level scheme, that the Nd ion occupies a single site of C_2 symmetry in this matrix. These spectroscopic data corroborate our previous conclusion (deduced from the analysis of the *x* rays): A structural local disorder exists which is associated with a random distribution of the Ag^+ and Nd^{3+} ions.

D. Magnetic property

Figure 3 compares the experimental and calculated average temperature dependence of the reciprocal magnetic susceptibility, χ^{-1}. Above 70 K, the experimental susceptibility follows a Curie–Weiss-type law with a calculated moment of $3.73\,\mu_B$ in agreement with the expected value, $3.6\,\mu_B$, for the free ion ground $^4\mathbf{I}_{9/2}$ of the Nd^{3+} ion. The evident deviation from linearity at low temperature reflects the splitting of the ground state under the influence of the crystal field. The observed slight discrepancy when the temperature increases could be related to a variation of the crystal field, usually assumed to be temperature independent since, in fact, the network parameters smoothly with the temperature.

ACKNOWLEDGMENT

The authors acknowledge financial support from the Spanish CYCIT Project No. MAT2000-0753-C02-02.

[1] C. C. Torardi, C. Page, L. H. Brixner, G. Blasse, and G. T. Dirksen, J. Solid State Chem. **69**, 171 (1987).
[2] J. P. M. Van Vliet, G. Blasse, and L. H. Brixner, J. Solid State Chem. **76**, 160 (1988).
[3] H. Yamamoto, S. Seki, and T. Ishiba, J. Solid State Chem. **94**, 396 (1991).
[4] F. N. Shi, J. Meng, and Y. F. Ren, J. Phys. Chem. Solids **59**, 105 (1997).
[5] T. F. Krueger and H. Mueller-Buschbaum, Z. Anorg. Allg. Chem. **617**, 79 (1991).
[6] H. Mueller-Buschbaum and O. Sedello, Z. Anorg. Allg. Chem. **620**, 647 (1994).
[7] H. Mueller-Buschbaum and H. Szillat, J. Alloys Compd. **204**, 231 (1994).
[8] H. Mueller-Buschbaum and O. Sedello, J. Alloys Compd. **204**, 237 (1994).
[9] S. Gallinat and Z. Naturforschung, Teil B. Anorg. Chem. **51**, 240 (1996).
[10] A. Boehlke and H. Mueller-Buschbaum, J. Less-Common Met. **162**, 141 (1990).
[11] H. Mueller-Buschbaum and H. Szillat, Z. Anorg. Allg. Chem. **620**, 642 (1991).
[12] H. Mueller-Buschbaum and T. Gressling, J. Alloys Compd. **202**, 63 (1993).
[13] P. V. Klevtsov, V. Y. Maksin, and R. F. Klevtsova, Kristallografiya **21**, 759 (1976).
[14] H. Mueller-Buschbaum and T. Gressling, J. Alloys Compd. **201**, 267 (1993).
[15] H. Mueller-Buschbaum and T. Krueger, Z. Anorg. Allg. Chem. **607**, 52 (1992).
[16] R. F. Klevtsova, L. A. Glinskaya, L. P. Kozeeva, and P. V. Klevtsov, Kristallografiya **17**, 768 (1972).
[17] A. W. Sleight, K. Aykan, and D. B. Rogers, J. Solid State Chem. **13**, 231 (1975).
[18] H. Li, G. Hong, and S. Yue, Zhongguo Xitu Xuebao **8**, 37 (1990).
[19] M. Rath and H. Mueller-Buschbaum, J. Alloys Compd. **198**, 237 (1994).
[20] F. Shi, J. Meng, and Y. Reng, J. Solid State Chem. **121**, 236 (1996).
[21] J. Rodriguez-Carvajal, *FULLPROF Program for Rietveld Refinement and Pattern Matching Analysis* (Lab. León Brillouin) (CEA-CNRS, Saclay, France, 1999).
[22] W. T. Carnall, G. L. Goodman, K. Rajnak, and R. S. Rana, J. Chem. Phys. **90**, 3443 (1989).
[23] B. G. Wybourne, *Spectroscopic Properties of Rare Earths* (Wiley, New York, 1965).
[24] C. Colón, A. Alonso-Medina, F. Fernández, A. Duran, and R. Barajas, *Proceeding of the 2000, Rencontre Franco-Spagnole* p. 14.
[25] P. Porcher (unpublished).
[26] J. H. Van Vleck, *The Theory of the Electric and Magnetic Susceptibilities* (Oxford University Press, London, 1932), p. 245.
[27] J. H. Van Vleck, J. Appl. Phys. **39**, 365 (1968).
[28] C. Cascales, R. Sáez Puche, and P. Porcher, J. Solid State Chem. **114**, 52 (1995).
[29] C. Cascales, R. Sáez Puche, and P. Porcher, Chem. Phys. **240**, 291 (1999).
[30] R. G. Brown, J. Denning, A. Hallet, and S. D. Ross, Spectrochim. Acta, Part A **26**, 963 (1970).
[31] H. M. Crosswhite and H. Crosswhite, J. Opt. Soc. Am. **1**, 246 (1984).